Exfoliated and Restacked MoS_2 and WS_2: Ionic or Neutral Species? Encapsulation and Ordering of Hard Electropositive Cations

Joy Heising and Mercouri G. Kanatzidis*

Contribution from the Department of Chemistry and Center for Fundamental Materials Research, Michigan State University, East Lansing, Michigan 48824

Received May 17, 1999

Abstract: The relationship between charge and structure in restacked MS_2 (M = Mo, W) has been probed by cation encapsulation and chemical oxidation and characterized by elemental analysis, electron diffraction, X-ray diffraction, and Differential Scanning Calorimetry. Alkali cations have been encapsulated in MoS_2 and WS_2 without the presence of a co-intercalated counterion, suggesting a negative charge in the 0.15−0.25 electrons per M atom range. Electron diffraction studies show ordering of these cations between the layers. Chemical oxidation with I_2 or Br_2 results in a change in the structure of restacked MoS_2, giving rise to a $\sqrt{3}a \times \sqrt{3}a$ superlattice, whereas no change is observed in the structure of restacked WS_2. Differential Scanning Calorimetry studies show that the irreversible exothermic transition to 2H-MS_2 shifts to lower temperature with oxidation. The observed structural distortion and residual negative charge uniquely explain the thermopower measurements, which indicate that restacked MoS_2 and WS_2 are p-type metallic conductors.

Introduction

2H-MoS_2 and 2H-WS_2 are the most stable members of the family of layered dichalcogenides, and find practical application in such processes as hydrodesulfurization (HDS) due to their availability and relatively low cost.[1] Both materials strongly resist attempts to incorporate guest species between their layers.[2] Li atoms can be inserted into MoS_2 (and WS_2) only upon treatment with very strong reducing agents such as *n*-butyllithium (*n*-BuLi) or $LiBH_4$.[3,4] $LiMoS_2$ and $LiWS_2$, however, exhibit a remarkable ability to exfoliate in water by the following redox reaction

$$LiMS_2 + H_2O \rightarrow (MS_2)_{\text{single layers}} + LiOH + H_2(g) \quad (1)$$

resulting in a colloidally dispersed suspension of single layers.[4,5] The layers can be recovered in a restacked form by filtration, centrifugation, or precipitation. The ability of these materials to exfoliate and to be restacked with relative ease has permitted the encapsulation of a wide variety of guest species which include neutral organic molecules,[6] polymers,[7] metal chalcogenide[8] and metal oxide[9] clusters, metallocenes,[10] porphyrins,[11] and metal cations.[12,13]

The authors who first reported the exfoliation of MoS_2 believed that the redox reaction between H_2O and MoS_2 resulted in complete oxidation of the layers, returning the molybdenum to a 4+ oxidation state, because many of the molecules which have been encapsulated are neutral.[6−8,14] A net drift of the suspended layers toward the anode in an electrophoresis apparatus was observed by these authors, but was attributed to OH^- ions associated with the layers which could be displaced by the organic molecules.[15] Subsequent pH studies seemed to support this hypothesis.[16] The increasing number of examples of cationic species which have been encapsulated have suggested to other authors that the layers may retain some negative charge.[8,10−13,17] It is rather curious that restacked MoS_2 (and WS_2) can incorporate both cationic and neutral species. The ambiguity of the situation stems from an abundance of both

(1) (a) Chianelli, R. R.; Daage, M.; Ledoux, M. J. *Adv. Catal.* **1994**, *40*, 177−232. (b) Daage, M.; Chianelli, R. R. *J. Catal.* **1994**, *149* (2), 414. (c) Daage, M.; Chianelli, R. R.; Ruppert, A. F.; Ledoux, M. J.; Massoth, F. S.; Breysse, M.; Niemantsverdriet, J. W.; Moulijn, J. A.; Iwamoto, R.; Grimblot, J.; Arnaud, Y.; Topsoe, H. *Stud. Surf. Sci. Catal.* **1993**, 75: 571. (d) Harris, S.; Chianelli, R. R. *J Catal* **1984**, *86* (2), 400.

(2) Whittingham, M. S. *Prog. Solid State Chem.* **1978**, *12*, 41−99.

(3) (a) Dines, M. B. *Mater. Res. Bull.* **1975**, *10*, 287. (b) Yang, D.; Frindt, R. F. *J. Phys. Chem. Solids* **1996**, *57*, 1113−1116.

(4) (a) Tsai, H. L.; Heising, J.; Schindler, J. L.; Kannewurf, C. R.; Kanatzidis, M. G. *Chem. Mater.* **1997**, *9*, 879. (b) Wang, L.; Kanatzidis, M. G. Manuscript in preparation.

(5) Joensen, P.; Frindt, R. F.; Morrison, S. R. *Mater. Res. Bull.* **1986**, *21*, 457−461.

(6) (a) Divigalpitiya, W. M. R.; Frindt, R. F.; Morrison, S. R. *Science* **1989**, *246*, 369. (b) Zhou, X.; Yang, D.; Frindt, R. F. *J. Phys. Chem. Solids* **1996**, *57*, 1137−1140. (c) Kosidowski, L.; Powell, A. V. *Chem. Commun.* **1998**, 2201−2202.

(7) (a) Divigalpitiya, W. M. R.; Frindt, R. F.; Morrison, S. R. *J. Mater. Res.* **1991**, *6*, 1103. (b) Kanatzidis, M. G.; Bissessur, R.; DeGroot, D. C.; Schindler, J. L.; Kannewurf, C. R. *Chem. Mater.* **1993**, *5*, 595. (c) Wang, L.; Schindler, J. L.; Thomas, J. A.; Kannewurf, C. R.; Kanatzidis, M. G. *Chem. Mater.* **1995**, *7*, 1753. (d) Ruiz-Hitzky, E.; Jimenez, R.; Casal, B.; Manriquez, V.; Santa Ana, A.; Gonzalez, G. *Adv. Mater.* **1993**, *5*, 738−741. (e) Lemmon, J. P.; Lerner, M. M. *Chem. Mater.* **1994**, *6*, 207−210.

(8) (a) Brenner, J.; Marshall, C. L.; Ellis, L.; Tomczyk, N.; Heising, J.; Kanatzidis, M. G. *Chem. Mater.* **1998**, *10*, 1244−1257. (b) Bissessur, R.; Heising, J.; Hirpo, W.; Kanatzidis, M. G. *Chem. Mater.* **1996**, *8*, 318.

(9) (a) Heising, J.; Bonhomme F.; Kanatzidis, M. G. *J. Solid State Chem.* **1998**, *139*, 22. (b) Ollivier, P. J.; Kovtyukhova, N. I.; Keller, S. W.; Mallouk, T. E. *Chem. Commun.* **1998**, 1563−1564.

(10) Tagaya, H.; Hashimoto, T.; Karasu, M.; Izumi, T.; Chiba, K. *Chem. Lett.* **1991**, 2113−2116.

(11) Nakagaki, S.; Mangrich, A. S.; Wypych, R. *Inorg. Chim. Acta* **1997**, *254*, 213−217.

(12) (a) Dungey, K. E.; Curtis, M. D.; Penner-Hahn, J. E. *J. Catal.* **1998**, *175*, 129. (b) Gee, M. A.; Frindt, R. F.; Morrison, S. R. *Mater. Res. Bull.* **1986**, *21*, 543.

(13) (a) Golub, A. S.; Shumilova, I. B.; Zubavichus, Y. V.; Jahncke, M.; Süss-Fink, G.; Danot, M.; Novikov, Y. N. *J. Mater. Chem.* **1997**, *7*, 163−167. (b) Danot, M.; Mansot, J. L.; Golub, A. S.; Protzenko, G. A.; Fabritchnyi, P. B.; Novikov, Y. N.; Rouxel, J. *Mater. Res. Bull.* **1994**, *29*, 833−841. (c) Golub, A. S.; Payen, C.; Protzenko, G. A.; Novikov, Y. N.; Danot, M. *Solid State Commun.* **1997**, *102*, 419−423.

(14) Divigalpitiya, W. M. R.; Frindt, R. F.; Morrison, S. R. *Appl. Surf. Sci.* **1991**, *48*−*49*, 572−575.

(15) Divigalpitiya, W. M. R.; Morrison, S. R.; Frindt, R. F. *Thin Solid Films* **1990**, *186*, 177−192.

(16) (a) Miremadi, B. K.; Morrison, S. R. *J. Appl. Phys.* **1988**, *63*, 4970. (b) Miremadi, B. K.; Cowan, T.; Morrison, S. R. *J. Appl. Phys.* **1991**, *69*, 6373. (c) Miremadi, B. K.; Morrison, S. R. *J. Appl. Phys.* **1990**, *67*, 1515.

10.1021/ja991644d CCC: $18.00
Published on Web 12/04/1999

Li^+ and OH^- generated in the exfoliation process: Li^+, which could counterbalance a negative charge on the layers when neutral species are intercalated, is a notoriously difficult element to detect; OH^-, which could co-intercalate with the cationic species, can be confused with residual co-intercalated H_2O.

In addition to the unresolved issues about the oxidation state of the layers, there has also been confusion about the atomic structure of the layers. Reduction of 2H-MoS_2 with *n*-BuLi or $LiBH_4$ results in a structural transformation in the layers, causing the geometry around the metal atoms to shift from trigonal prismatic to octahedral.[18] This results in a change in the conductive properties of the material from semiconducting to metallic.[18,19] This structural change appears to be retained in exfoliated MoS_2, with a structural distortion that results in a $\sqrt{3}a \times a$ orthorhombic superlattice.[20,21] Restacked MoS_2 has also been called 1T-MoS_2 because of the octahedral coordination of the Mo atom. Restacked WS_2 appears to be analogous to restacked MoS_2.[4,21] Another material that has been called 1T-MoS_2 is prepared by high-temperature synthesis and subsequent oxidation of $K_{0.33}(H_2O)_yMoS_2$.[22] Restacked MoS_2 and 1T-MoS_2 were thought to be the same material because both appear to have octahedral metal coordination and both undergo an irreversible exothermic transition to 2H-MoS_2 at around 100 °C.[22,23] 1T-MoS_2, however, exhibits a $\sqrt{3}a \times \sqrt{3}a$ superlattice.[22,24] The $\sqrt{3}a \times a$ superlattice found in restacked MoS_2 is due to M−M associations resulting in the formation of zigzag chains,[21] whereas a $\sqrt{3}a \times \sqrt{3}a$ superlattice would involve M−M trimerization.

Are these layers neutral or charged? Why do 1T-MoS_2 and restacked MoS_2 have different superlattices? What is the impact of negative charge on the structure of these materials? If the MoS_2 layers are slightly reduced, how does it affect the electrical conductivity? In this paper we describe our experimental efforts toward answering these questions. The encapsulation of hard, electropositive alkali metal cations was used as a primary tool, and these were chosen due to their relatively poor affinity for OH^-, which make them perhaps the best species for chemical analyses to determine negative charge. The materials were characterized by X-ray diffraction, electron diffraction, DTA, and elemental analyses. The treatment of $LiMS_2$ and exfoliated MS_2 with the oxidizing agent Br_2 and concentrated HCl has also been conducted and the products characterized by X-ray diffraction, electron diffraction, and DSC measurements. The structural conclusions presented are supported by thermopower measurements of restacked MoS_2 and WS_2, which address the effects of structure and charge on the nature of their electrical conductivity.

Experimental Section

$LiMoS_2$ and $LiWS_2$ were synthesized by the $LiBH_4$ method.[4] MoS_2 was purchased from Cerac. WS_2 was purchased from Alfa Aesar. $LiBH_4$, acetonitrile, RbCl, CsF, and CsI were purchased from Aldrich. KCl and $BaCl_2 \cdot 2H_2O$ were purchased from J. T. Baker. Br_2 and NaCl were purchased from EM Science. I_2 was purchased from Mallinckrodt. HCl was purchased from Columbus Chemical Industries. All compounds were used as received.

MoS_2 Aqueous Suspension. In a glovebox under nitrogen atmosphere $LiMoS_2$ (0.1 g, 0.6 mmol) was placed in a 125 mL Erlenmeyer flask equipped with a stir bar and rubber stopper. The flask was removed from the glovebox and 10 mL of deoxygenated deionized H_2O was added. The mixture was allowed to stir for 0.5 h, then the contents of the flask were transferred to a centrifuge tube and centrifuged for 0.5 h. The supernatant was decanted (pH >12) and to the black gooey solid at the bottom of the tube 10 mL of fresh deoxygenated deionized H_2O was added to rinse away the LiOH. The tube was agitated to resuspend the product, and the mixture again centrifuged for 0.5 h. This rinsing was conducted three times, the supernatant having pH ∼12, ∼9, and ∼7 after each rinse. Then 10 mL more deoxygenated deionized H_2O was added, the tube was agitated to resuspend the product, and the contents of the centrifuge tube were returned to a 125 mL Erlenmeyer flask with a stir bar. The suspension was stirred for at least 0.5 h before further use.

WS_2 Aqueous Suspension. In a glovebox under nitrogen atmosphere $LiWS_2$ (0.1 g, 0.39 mmol) was placed in a 125 mL Erlenmeyer flask equipped with stir bar and rubber stopper. The flask was removed from the glovebox and 10 mL of deoxygenated deionized H_2O was added. The material was then centrifuged, rinsed, and resuspended in the same manner as MoS_2.

$A_x(H_2O)_yMoS_2$ (Na, K, Rb). The alkali chloride salt (1.8 mmol) was dissolved in ∼2−4 mL of H_2O. To this solution was added an aqueous suspension of MoS_2 (3:1 excess A^+). Flocculation occurred immediately. The reaction mixture was stirred for one-half hour and centrifuged and the supernatant decanted. The product was rinsed and centrifuged three times as described in the preparation of aqueous MoS_2, then deposited on a glass slide until dry. Formulas for the products were determined to be $Na_{0.14}(H_2O)_{0.45}MoS_2$, $K_{0.23}(H_2O)_{0.4}MoS_2$, $Rb_{0.15}(H_2O)_{0.3}MoS_2$, and $Cs_{0.23}(H_2O)_yMoS_2$. In the Cs case CsF was used.

$Ba_x(H_2O)_yMoS_2$. $BaCl_2 \cdot 2H_2O$ (0.88 g, 3.6 mmol) was dissolved in ∼5 mL of H_2O. To this solution was added an aqueous suspension of MoS_2 (6:1 excess Ba^{2+}). Flocculation occurred immediately. The product isolation was analogous to that used for $A_x(H_2O)_yMoS_2$.

$A_x(H_2O)_yWS_2$ (Na, K). The alkali chloride salt (2.4 mmol) was dissolved in ∼3−5 mL of H_2O. To this solution was added an aqueous suspension of WS_2 (6:1 excess Na^+). Flocculation occurred immediately. The product isolation was analogous to that used above.

$Rb_{0.24}(H_2O)_{0.34}WS_2$. RbCl (0.15 g, 1.2 mmol) was dissolved in ∼3.5 mL of H_2O. To this solution was added an aqueous suspension of WS_2 (3:1 excess Rb^+). Flocculation occurred immediately. The product isolation was analogous to that above.

$Cs_{0.13}(H_2O)_yWS_2$. An aqueous suspension of WS_2 was added to 5 mL of a concentrated CsF solution in H_2O (or 5 mL of CsI (2.8 mmol) in water) (7:1 excess Cs^+). Flocculation occurred immediately. The product isolation was analogous to that given above.

$Ba_{0.08}(H_2O)_yWS_2$. $BaCl_2 \cdot 2H_2O$ (0.29 g, 1.2 mmol) was dissolved in ∼5 mL of H_2O. To this solution was added an aqueous suspension of WS_2 (3:1 excess Ba^{2+}). Flocculation occurred immediately. The product isolation was analogous to that used above.

H_xMoS_2. In a glovebox under nitrogen atmosphere $LiMoS_2$ (0.3 g, 1.8 mmol) was placed in a 125 mL Erlenmeyer flask equipped with a stir bar and rubber stopper. The flask was removed from the glovebox and 30 mL of cold concentrated HCl was added. The reaction mixture was stirred briefly, then centrifuged for a few minutes. The supernatant was decanted, then 30 mL of cold H_2O was added to the solid to rinse,

(17) (a) Golub, A. S.; Protsenko, G. A.; Gumileva, L. V.; Buyanovskaya, A. G.; Novikov, Y. N. *Russ. Chem. Bull*. **1993**, *42*, 632−634. (b) Golub, A. S.; Shumilova, I. B.; Novikov, Y. N.; Mansot, J. L.; Danot, M. *Solid State Ionics* **1996**, *91*, 307−314.

(18) (a) Py, M. A.; Haering, R. R. *Can. J. Phys*. **1983**, *61*, 76. (b) Mulhern, P. J. *Can. J. Phys*. **1989**, *67*, 1049−1052.

(19) Bissessur, R.; Kanatzidis, M. G.; Schindler, J. L.; Kannewurf, C. R. *J. Chem. Soc., Chem. Commun.* **1993**, 1582.

(20) (a) Yang, D.; Sandoval, S. J.; Divigalpitiya, W. M. R.; Irwin, J. C.; Frindt, R. F. *Phys. Rev. B* **1991**, *43*, 12053−12056. (b) Joensen, P.; Crozier, E. D.; Alberding, N.; Frindt, R. F. *J. Phys. Solid State Phys*. **1987**, *20*, 4043−4053. (c) Qin, X. R.; Yang, D.; Frindt, R. F.; Irwin, J. C. *Ultramicroscopy* **1992**, *42*−*44*, 630−636. (d) Qin, X. R.; Yang, D.; Frindt, R. F.; Irwin, J. C. *Phys. Rev. B* **1991**, *44*, 3490−3493. (e) Sandoval, S. J.; Yang, D.; Frindt, R. F.; Irwin, J. C. *Phys. Rev. B* **1991**, *44*, 3955−3962.

(21) Heising, J.; Kanatzidis, M. G. *J. Am. Chem. Soc*. **1999**, *121*, 638−643.

(22) (a) Wypych, F.; Schöllhorn, R. *J. Chem. Soc., Chem. Commun*. **1992**, 1386−1388. (b) Wypych, F.; Solenthaler, C.; Prins, R.; Weber, Th. *J. Solid State Chem.* **1999**, *144*, 430. (c) Schöllhorn, R.; Kümpers, M.; Plorin, D. *J. Less-Common. Metals* **1978**, *58*, 55.

(23) (a) Yang, D.; Frindt, R. F. *Mol. Cryst. Liq. Cryst*. **1994**, *244*, 355−360. (b) Bissessur, R.; Kanatzidis, M. G.; Schindler, J. L.; Kannewurf, C. R. *J. Chem. Soc., Chem. Commun*. **1993**, 1582−1585.

(24) Wypych, F.; Weber, Th.; Prins, R. *Chem. Mater*. **1998**, *10*, 723−727.

and the slurry was centrifuged again. This rinsing was repeated two more times, the supernatant after each rinse having pH ~1, ~1, and ~7, respectively. The solid was then slurried in a few milliliters of H_2O and deposited on a glass slide to dry overnight.

H_xWS_2. In a glovebox under nitrogen atmosphere $LiWS_2$ (0.3 g, 1.2 mmol) was placed in a 125 mL Erlenmeyer flask equipped with a stir bar and rubber stopper. The reaction procedure and rinsing was the same as the one used to prepare H_xMoS_2, with the supernatant after each rinse having pH ~1, ~4, and ~7, respectively. The solid was then slurried in a few milliliters of H_2O and deposited on a glass slide to dry overnight.

Oxidized $LiMoS_2$. (a) Method 1. In a glovebox under nitrogen atmosphere $LiMoS_2$ (0.3 g, 1.8 mmol) was placed in a 125 mL Erlenmeyer flask equipped with a stir bar and rubber stopper. The flask was removed from the box, and 50 mL of a 0.18 M solution of I_2 in acetonitrile or 50 mL of a 45 mM solution of Br_2 in acetonitrile was added to the solid (5:1 excess I_2/Br_2). The mixture was stirred for different amounts of time ranging from 15 min to 4 days, then was centrifuged and the supernatant decanted. The product was rinsed by resuspending it in 15 mL of acetonitrile and recentrifuging 2 times and then deposited on a glass slide and a Saran wrapped transmission XRD slide to dry.

(b) Method 2. An exfoliated suspension of MoS_2 was prepared as described previously from $LiMoS_2$ (0.15 g, 0.9 mmol), then centrifuged and rinsed once with acetonitrile. The rest of the procedure is the same as in method 1 above.

Oxidized $LiWS_2$. (a) Method 1. In a glovebox under nitrogen atmosphere $LiWS_2$ (0.3 g, 1.2 mmol) was placed in a 125 mL Erlenmeyer flask equipped with a stir bar and rubber stopper. The flask was removed from the box, and to the solid 50 mL of a 0.12 M MeCN solution of I_2 or the corresponding 75 mL of a 80 mM MeCN solution of Br_2 was added 10:1 excess I_2/Br_2. The mixture was stirred for varying amounts of time from ~15 min to a week and centrifuged and the supernatant decanted. The product was isolated as described for oxidized $LiMoS_2$.

(b) Method 2. An exfoliated suspension of WS_2 was prepared as described previously from $LiWS_2$ (0.15 g, 0.6 mmol), then centrifuged and rinsed with acetonitrile. The rest of the procedure is the same as in method 1 above.

(c) Method 3. $LiWS_2$ (0.15 g, 0.6 mmol) was used to prepare an exfoliated suspension as described previously. Next 100 mL of a saturated aqueous solution of Br_2 was added. The product was centrifuged immediately for a few minutes, then rinsed with water and centrifuged three times. It was deposited on a glass slide and a Saran wrapped transmission XRD slide to dry.

Characterization. Selected area electron diffraction patterns were collected using a JEOL 120 CX transmission electron microscope (TEM). Transmission and reflection powder X-ray diffraction patterns were collected using a Rigaku-Denki/RW400F2 (Rotaflex) rotating anode X-ray diffractometer using Cu Kα radiation. Differential scanning calorimetry (DSC) measurements were conducted using a Shimadzu DSC-50 instrument under nitrogen flow in sealed aluminum containers at a heating rate of 5 deg C/min. Thermogravimetric analyses (TGA) employed a Shimadzu TGA-50 instrument under nitrogen flow in quartz containers at a heating rate of 2 deg C/min. Energy dispersive spectroscopy (EDS) was used to determine the alkali metal to Mo/W ratio, and a JEOL-JSM-6400V scanning electron microscope was operated at an accelerating voltage of 30 kV using a Tracor Northern 5500 X-ray microanalysis attachment. Thermopower measurements were made with a MMR Technologies Seebeck System.

Results and Discussion

Cation-Encapsulated MS_2. Addition of exfoliated MoS_2/WS_2 to the alkali halide solution results in immediate flocculation of the suspension. This rapid precipitation, which is not usually observed upon addition of neutral species, strongly suggests that the interaction of the layers with the alkali cations is ionic in nature. Similar behavior is observed upon addition of exfoliated MoS_2/WS_2 to solutions containing $Al_{13}O_4(OH)_{24}(H_2O)_{12}^{7+}$ or tetraphenylphosphonium cations.[9a,25]

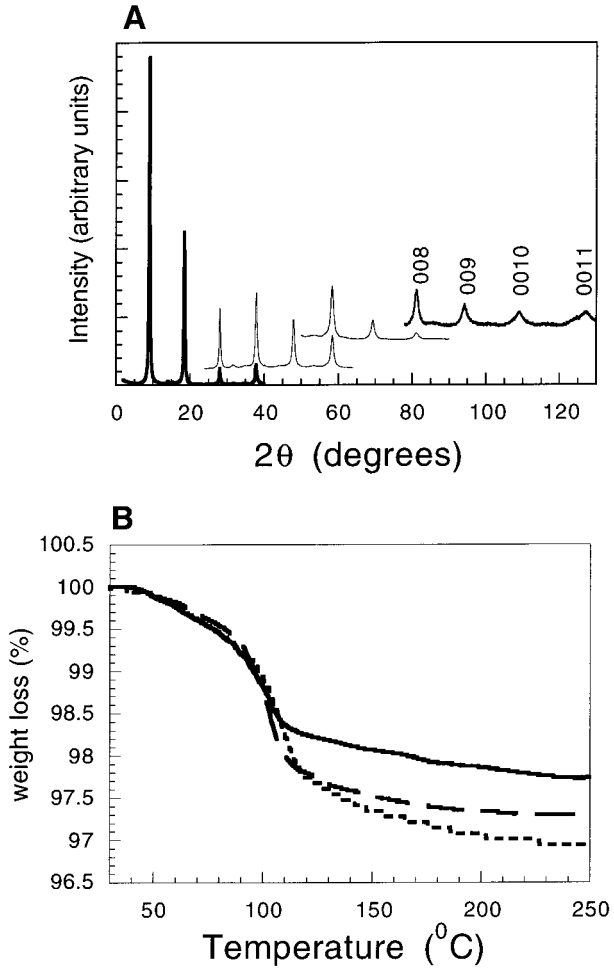

Figure 1. (A) Reflectance X-ray diffraction pattern of $Na_{0.18}(H_2O)_{0.45}WS_2$. The 00*l* reflections predominate, exhibiting a *d* spacing of 9.7 Å which corresponds to an expansion of 3.5 Å. (B) TGA of $Na_{0.18}(H_2O)_{0.45}WS_2$ (dotted line), $K_{0.21}(H_2O)_{0.40}WS_2$ (dashed line), and $Rb_{0.24}(H_2O)_{0.34}WS_2$ (solid line). Weight loss corresponds to the loss of co-encapsulated H_2O.

The samples were characterized by reflectance X-ray diffraction (Figure 1a) and were found to be well ordered, particularly compared to the patterns of samples containing neutral species such as the $Co_6S_8L_6$ clusters.[8] The predominance of the 00*l* reflections in the pattern is due to the tendency of lamellar materials to adopt a preferred orientation. All samples exhibited interlamellar *d* spacings in the range 9.3−9.7 Å (3.1−3.5 Å expansion), indicating co-encapsulation of approximately one monolayer of water.

The flocculated products were found to have the following formulas: $Na_{0.14}(H_2O)_xMoS_2$, $K_{0.23}(H_2O)_xMoS_2$, $Rb_{0.15}(H_2O)_xMoS_2$, $Cs_{0.23}(H_2O)_xMoS_2$, $Na_{0.18}(H_2O)_xWS_2$, $K_{0.21}(H_2O)_xWS_2$, $Rb_{0.24}(H_2O)_xWS_2$, $Cs_{0.13}(H_2O)_xWS_2$, and $Ba_{0.08}(H_2O)_xWS_2$. Thermogravimetric analysis, performed to determine the amount of co-encapsulated water, indicates a range of 0.3−0.45 for *x* (Figure 1b). Higher *x* values were found for samples containing Na^+ and K^+ and lower values for those containing Cs^+ and Rb^+. No halide counterions were detected. Although the presence of OH^- ions cannot be completely discounted, the pH of the suspension (~7) and the relatively poor affinity of the alkali cations for OH^- ions make their co-encapsulation unlikely.

(25) Heising, J.; Kanatzidis, M. G. Unpublished results.

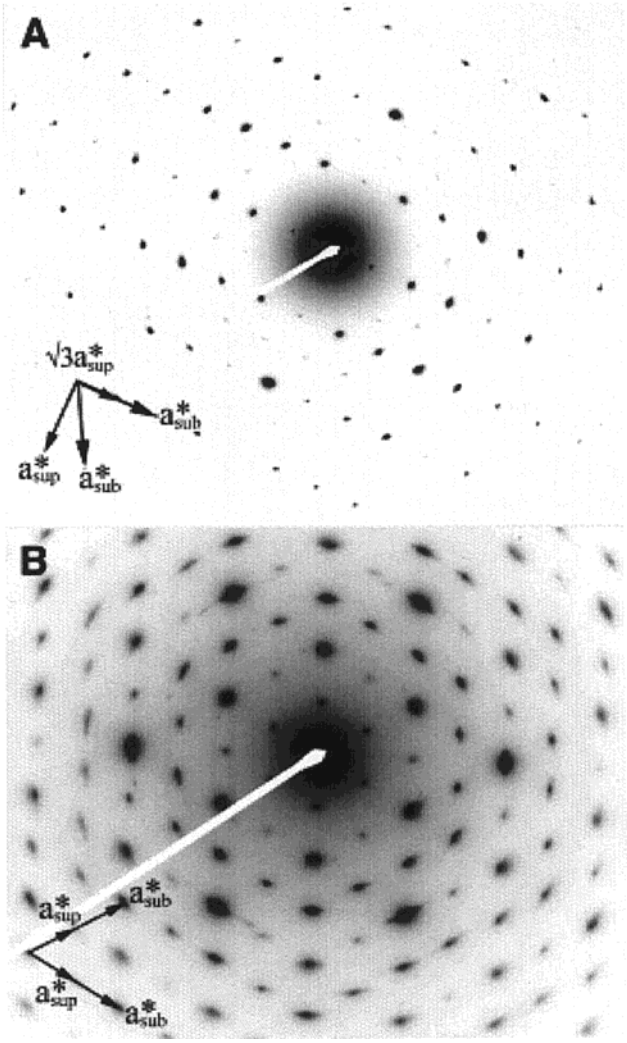

Figure 2. Selected area electron diffraction (SAED) patterns of (A) a thin crystal and (B) a thick crystal of restacked WS_2. Twinning of the orthorhombic $\sqrt{3}a \times a$ superlattice gives rise to a pseudohexagonal $2a \times 2a$ superlattice.

Electron Diffraction Studies of Alkali Cation Encapsulated MS_2. The cation intercalated MoS_2 and WS_2 samples were also examined by electron diffraction. Both restacked MoS_2 and WS_2 give rise to electron diffraction patterns which appear to be more simple than they actually are.[21] Recently, we solved and refined the structure of restacked MoS_2 and WS_2 from electron diffraction data.[21] The materials exhibit a superlattice caused by metal−metal associations to form zigzag chains, similar to those observed in WTe_2.[26] This zigzag distortion results in the doubling of one axis of the hexagonal sublattice. As the hexagonal symmetry is destroyed, the new lattice is best described by an $\sqrt{3}a \times a$ orthorhombic cell (Figure 2a). Due to their turbostratic nature and the disorder introduced by the exfoliation/flocculation process, the diffraction patterns of exfoliated and restacked MoS_2 and WS_2 are often a "triplet" of these orthorhombic cells, forming an apparent $2a \times 2a$ superlattice (Figure 2b). Failure to recognize this twinning can lead to incorrect interpretations of the M−M interactions.

The cation intercalated samples are represented by an array of diffraction patterns (Figures 3, 4, and 6) which contain an *additional superlattice* due to ordering of the electropositive cations in the gallery. The high vacuum found in a TEM ($\sim 10^{-7}$ Torr) probably results in the removal of most of the co-encapsulated water from the samples. The majority of the patterns appear at first glance to contain a weak $6a \times 6a$ superlattice relative to the hexagonal sublattice, with distinct variations in the reflections present and the intensity distribution from one pattern to the next. Because of the propensity of these materials for twinning, however, the diffraction patterns are actually quite complicated.

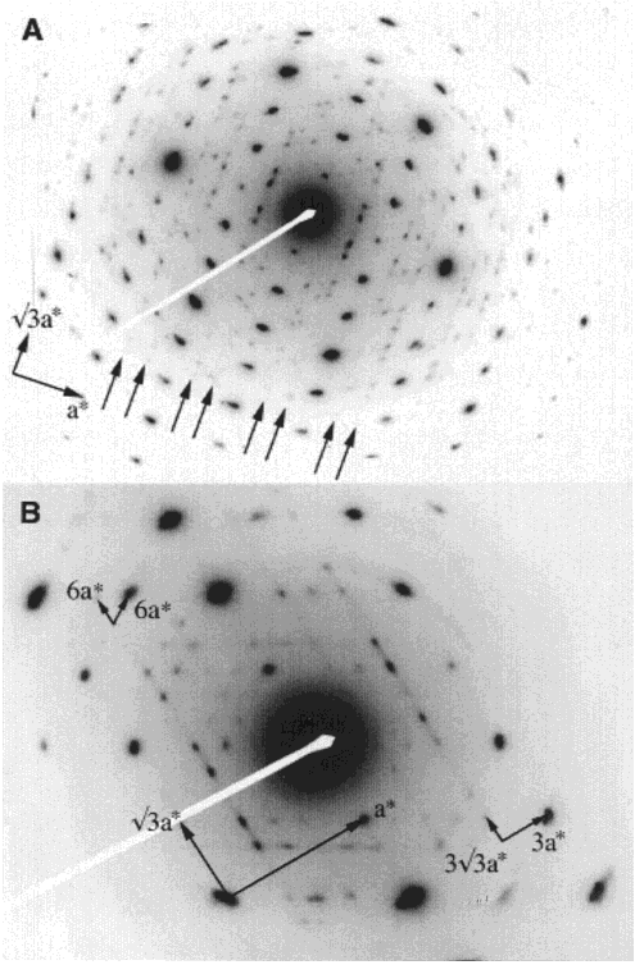

Figure 3. SAED patterns of (A) $Cs_{0.23}MoS_2$ and (B) $Cs_{0.13}WS_2$. Superlattice reflections caused by ordering of the Cs^+ ions are spaced in thirds between the columns of host−lattice reflections along the $\sqrt{3}a^*$ axis, indicating a tripling of the *a* axis. Examination of one of these columns of superlattice reflections reveals a tripling of the $\sqrt{3}a$ axis as well, resulting in a $3\sqrt{3}a \times 3a$ supercell. Twinning of the host-lattice projects a pseudo $6a \times 6a$ unit cell.

Considering only the orthorhombic lattice caused by the formation of zigzag M−M chains in the host material,[21] Figures 3a and 3b contain one dominant $\sqrt{3}a \times a$ orthorhombic cell with only weak twinning. In the interest of clarity, this $\sqrt{3}a \times a$ orthorhombic lattice will henceforth be called the "host-lattice". A closer examination of Figure 3a reveals that the superlattice caused by the intercalated cations forms strong columns of reflections along the $\sqrt{3}a^*$ axis of the host-lattice. The superlattice reflections are spaced in thirds between the host-lattice reflections. This suggests that at least one cell parameter should be 3*a*. The reflections at 1/2 the spacing between the columns of host-lattice reflections can be attributed to the weak twinning of the host-lattice; thus, the same phenomena which give rise to a false $2a \times 2a$ lattice also give rise to a false 6*a* superlattice parameter. Interestingly, there do not appear to be

(26) (a) Brown, B. E. *Acta Crystallogr.* **1966**, *20*, 268. (b) Mar, A.; Jobic, S.; Ibers, J. A. *J. Am. Chem. Soc.* **1992**, *114*, 8963.

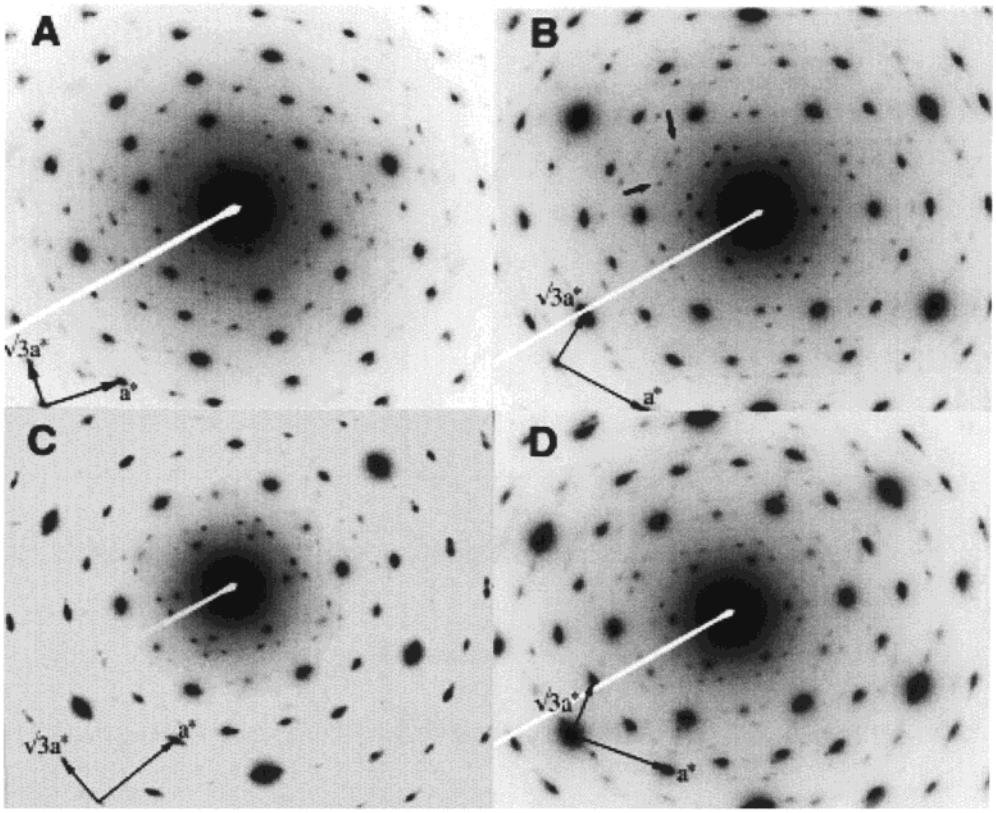

Figure 4. SAED patterns of (A) $K_{0.23}MoS_2$, which resembles the patterns in Figure 3, but the degree of twinning is slightly greater; (B) $K_{0.23}MoS_2$ and (C) $Rb_{0.15}MoS_2$, in which the host-lattice is more twinned but the crystals are still relatively thin; and (D) $K_{0.23}MoS_2$, from a thick crystal with a very twinned host-lattice and a "halo" of cation superlattice reflections. As twinning of the host-lattice increases, twinning of the cation superlattice increases, leading to a variety of diffraction patterns.

any superlattice reflections from the cations contained in the columns or rows of host-lattice reflections in Figure 3a. Considering one of the columns of superlattice reflections to find the second cell parameter, the smallest distance between two reflections is 1/3 the length of the (010) reflection of the host-lattice; therefore, the superlattice may be minimally described by the orthorhombic cell $3a' \times 3b$ relative to the host-lattice ($a' = \sqrt{3}a$), and $3\sqrt{3}a \times 3a$ (orthorhombic) relative to the hexagonal sublattice of the host material (Figure 3b).

It is logical to conclude that, if the host-lattice is somewhat twinned, the superlattice will be similarly twinned. In this manner the variations in the other diffraction patterns (Figure 4) can be explained by the degree of twinning of the $\sqrt{3}a \times a$ orthorhombic host-lattice and the $3a' \times 3b$ cation superlattice. Figure 4a is very similar to Figures 3a and 3b, but comes from $K_{0.23}MoS_2$ rather than $Cs_{0.23}MoS_2$ (Figure 3a) or $Cs_{0.13}WS_2$ (Figure 3b). The host-lattice is more twinned than the pattern in Figure 3a, but the pattern of cation ordering is essentially the same. Figures 4b and 4c are from crystals of $K_{0.23}MoS_2$ and $Rb_{0.14}$ MoS_2, respectively, that are twinned but are still relatively thin. The distribution of orthorhombic host-lattice cells is uneven, appearing to be stronger in one direction. Consequently, the cation superlattice in these pictures is still stronger in one direction, but does show evidence of twinning. Unlike the previous patterns, the cation superlattice reflections are now found in the columns of reflections along the $\sqrt{3}a^*$ axis of the dominant orthorhombic host-lattice (arrows, Figure 4b). This seems to be due to cation superlattices associated with the other (weaker) host-lattice cells. Figure 4d, on the other hand, came from a thicker crystal of $K_{0.23}MoS_2$. In this case, the twinning of the host-lattice is so pronounced that the host material exhibits the pseudo $2a \times 2a$ hexagonal lattice which is common in thicker crystals. The crystal is thin enough that the superlattice from the intercalated cations is still visible, but extremely weak. It is twinned in the same manner as the host-lattice, creating a hexagonal "halo" around the pseudo $2a \times 2a$ lattice. The systematic absences of the superlattice (for example, the 200, 130, and the 310) are completely destroyed due to the twinning, generating the pseudo $6a \times 6a$ cation superlattice.

Not all crystals gave rise to well-ordered cation superlattices. Crystals which contain discrete superlattice spots are somewhat unusual; more common are patterns which contain disorder or streaking along the $\sqrt{3}a^*$ axis of the host lattice.

Modeling the Cation Ordering. It is virtually impossible to obtain a diffraction pattern that is completely "single crystal" with respect to the host-lattice and the cation superlattice so that this manner of indexing the patterns might be confirmed; however, it is the best available indexing that can account for the variations in intensities and reflections from one diffraction pattern to the next, all of which can be found within one sample. As such, we have developed a cation ordering model from which an electron diffraction pattern was simulated. It has been designed to resemble the diffraction patterns in Figures 3a, 3b, and 4a, since they are the closest to a "single crystal" pattern (Figure 5). As noted previously, no superlattice reflection is found within a column or row of host-lattice reflections (Figure 3a). The model of cation ordering, depicted in Figure 5a, gives rise to such an electron diffraction pattern (Figure 5b).[27] The cell contains three chains. Alkali cations are placed along the

(27) Twinning of the host-lattice has been included in the simulation of the diffraction patterns in Figures 5b and 7b to give rise to patterns which better resemble the experimental data. For clarity, the M−M (M = Mo, W) zigzag chains of these other cells, which would be rotated 120° relative to one another, have been omitted from Figures 5a and 7a.

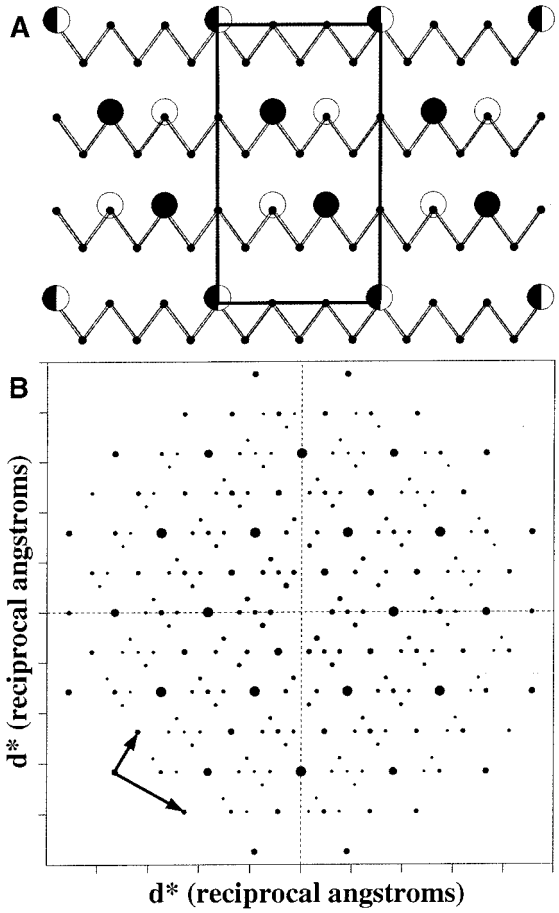

Figure 5. (A) Structural model and (B) simulated electron diffraction pattern to explain the observed SAED patterns in Figures 2−4. Filled circles represent cations in one layer; open circles represent cations in a second layer. The projection of the two layers results in a $3\sqrt{3}a \times 3a$ supercell.

chains in pockets defined by sulfur atoms, where a cation would be expected to reside in the gallery. One-third of the sites are empty in two of the chains; two-thirds of the sites are empty in the third chain. So many alkali cations would not normally be in such close proximity to one another within one layer, however, particularly when one considers the elemental analyses of these samples. More likely this picture represents the superposition of two alternating layers of cations, depicted as white and black. Hence, four of the cations have an occupancy of 0.5 and one cation is fully occupied. This results in a stoichiometry of $A_{0.167}MS_2$, which is consistent with the experimentally determined formula.

It is a necessary condition of the systematic absences that all the alkali cations be in the same kind of site, either "down" or "up" relative to the zigzag chain. The alkali cations occupy only sites which are pointing "up" in the model presented in Figure 5a; however, the sites which are pointing "down" are equally valid sites, so it becomes apparent that this is a possible source of disorder in the samples. The fact that there seems to be no disorder along the *a* axis indicates that the cations are better ordered along the zigzag chains than between zigzag chains.

A few of the electron diffraction patterns did not have this $3a \times 3b$ superlattice, but had a rather different pattern (Figure 6) corresponding to a $\sqrt{3}a \times \sqrt{3}a$ lattice combined with the pseudo $2a \times 2a$ lattice of the host material, forming a "honeycomb" pattern. The projection of this $\sqrt{3}a \times \sqrt{3}a$ unit cell occupies a smaller area than the previous superlattice (31 Å^2 vs 161 Å^2), which is puzzling when one considers that it is

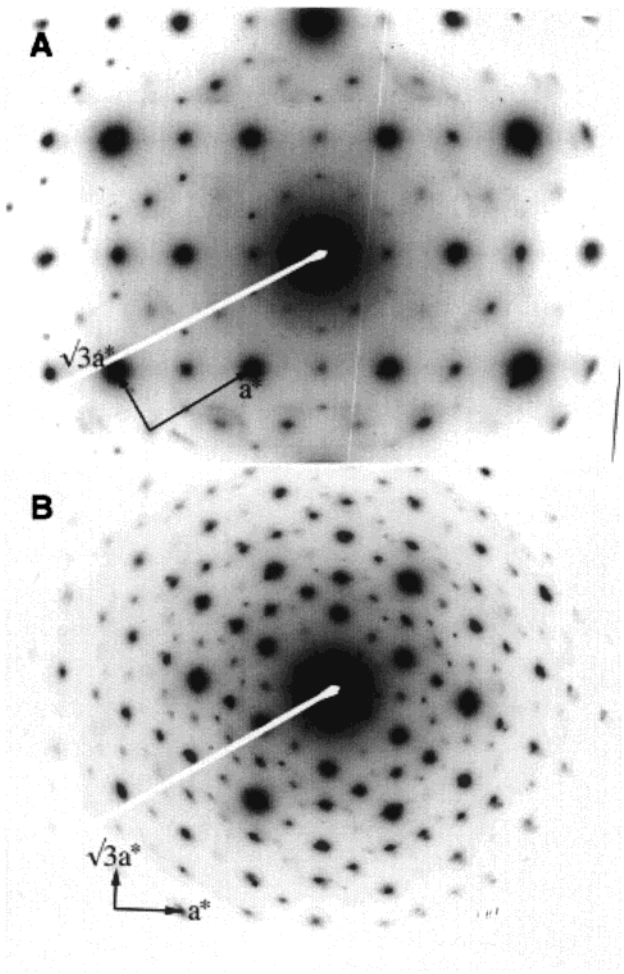

Figure 6. SAED patterns of (A) $Ba_{0.08}MoS_2$ and (B) $Na_{0.14}MoS_2$. The combination of a $\sqrt{3}a \times \sqrt{3}a$ cation superlattice with the pseudo $2a \times 2a$ host-lattice gives rise to a "honeycomb" pattern. This alternate cation superlattice, although most common for samples with encapsulated Ba^{2+}, could also be observed within samples which exhibited the $3\sqrt{3}a \times 3a$ superlattice.

most readily observed for samples in which Ba^{2+} is encapsulated. To reconcile such a lattice with the observed loading of cation one must again employ alternating layers of cations and consider their projection onto the *ab* plane. For example, in Figure 7a a model has been constructed with four layers of cations, depicted as white, black, gray, and striped circles. The unit cell per MS_2 layer is $2\sqrt{3}a \times 2\sqrt{3}a$ (solid line), but the projection is the smaller $\sqrt{3}a \times \sqrt{3}a$ lattice (dashed line). This gives a stoichiometry of $A_{0.09}MS_2$. The simulated diffraction pattern generated from this cation model (Figure 7b) resembles the experimental data.[27] It is now possible to understand why cations of different charge can have the same diffraction pattern: they can occupy half as many sites and require twice as many layers to project the appropriate unit cell. This is consistent with the fact that the superlattice is weaker in the samples containing Ba^{2+} than it is in the samples containing Na^+ or Rb^+.

Oxidation State of M (M = Mo,W) and the Charge of the Layers. The fact that one can see ordering of alkali cations in the MoS_2 and WS_2 layers without co-intercalation of the halide counterions supports the conclusion that the exfoliated and restacked layers retain residual negative charge. The layers in suspension behave as if they are solvated macroanions, precipitating readily in the presence of most cationic species.

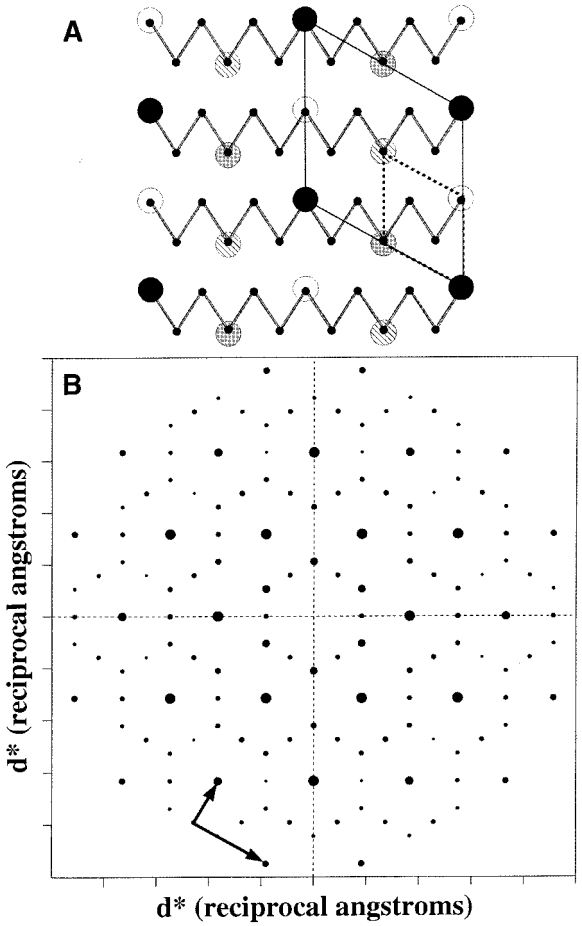

Figure 7. (A) Structural model and (B) simulated electron diffraction pattern to explain the observed SAED patterns in Figure 6. The black circles represent one layer of cations; the open circles a second; the gray circles a third; and the striped circles a fourth layer. Each layer contains a $2\sqrt{3}a \times 2\sqrt{3}a$ lattice (solid line), but the $\sqrt{3}a \times \sqrt{3}a$ superlattice is formed by the projection of the four layers (dashed line).

The hypothesis that the charge is due to the association of OH^- ions with the basal planes seems unlikely because the driving force for the association of the OH^- ions with the layers is not obvious. Furthermore, the pH of the exfoliated suspension has been reduced to ~7 by repeated rinsing. It seems surprising that any remaining OH^- ions would not be at least partially displaced in a solution with an excess of halide ions, resulting in materials with co-encapsulated halide ions. Unfortunately the high degree of disorder and the propensity of the systems for twinning make it impossible to determine the degree of negative charge on the layers based on the cell parameters of the samples with encapsulated cations.

The amount of negative charge on exfoliated and restacked MoS_2 has been studied rather extensively by a group of Russian scientists.[13,17] They assert that MoS_2 which has been freshly exfoliated under an inert atmosphere has a negative charge of approximately 0.15−0.29 per Mo atom (Li^+ counterion), but if the dispersion is allowed to sediment over time the value decreases to 0.07−0.12 per Mo atom.[17a] This slow, continuous oxidation of MoS_2 suspensions in solution over time may explain how it is possible to intercalate the neutral cobalt chalcogenide clusters, which require stirring for at least 2 days before encapsulation is observed.[8] This same group has also observed that in some transition metal systems it is possible to co-intercalate OH^- anions, thereby increasing the number of cations which may be encapsulated between the layers beyond the range of negative charge attributed to MoS_2.[13c] The ability of MoS_2 and WS_2 to accept co-intercalated OH^- ions hinders the quantitation of the negative charge through chemical analyses, as the exfoliation process creates an abundance of OH^- ions. These difficulties necessitate the use of "innocent" cations such as alkali metals, as they have poor affinity for OH^-. This is particularly true for the heavier alkali cations Rb^+ and $Cs,^+$ and they are easier to quantify than Li^+, Na^+, or K^+. Although the external OH^- ions can largely be removed by rinsing, it is difficult to be certain of their total removal without acidification of the solution. This complicates the situation by increasing the ionic strength of the solution and providing protons, a competing cation that is virtually impossible to unambiguously detect. In addition, if the MoS_2 is in fact slowly oxidized further in solution over time, more OH^- ions will be generated. Even restacked MoS_2 or MoS_2 with encapsulated hydrated alkali cations may continue to undergo redox chemistry with intercalated H_2O (see eq 1). Presumably the cations/OH^- pairs would remain trapped between the layers, indicating at least the oxidation state at the time of flocculation, but would not reflect the continuum of oxidation states possible for the material over time.

The results of our chemical analyses, which indicate a negative charge in the range 0.10−0.25 per Mo/W atom, are consistent with the results of the analysis of fresh Li^+ encapsulated samples[13,17] and are more reliable due to the use of the heavier alkali metal cations. Other studies involving the selective encapsulation of heavy metal ions such as Ag^+ and Pb^{2+} into MoS_2 and WS_2 have been conducted, and the results indicate a higher negative charge (0.5−0.8 per Mo/W atom).[28] These chalcophilic cations, like the alkali cations, have a poor affinity for OH^-; however, the samples have been prepared under different experimental conditions, in which the cations were inserted under anaerobic conditions in acidic solutions of moderate ionic strength, inhibiting the formation of colloidal suspension. These results suggest that the continuum of oxidation states possible for MoS_2 and WS_2 is much greater than the range reported in previous studies. The range of negative charge on the MS_2 layers which we observe is comparable to the range of charge observed in smectite clays, which is not surprising given the similarities in their behavior in aqueous conditions.[29]

Oxidation Reactions of $LiMS_2$. In light of increasing evidence that these materials have a negative charge, $LiMS_2$ and exfoliated MS_2 were treated with oxidizing agents to see if truly neutral MS_2 could be obtained by oxidizing with I_2 or Br_2 according to

$$Li_xMS_2 + I_2 \rightarrow MS_2 + xLiI \qquad (2)$$

The oxidized products were characterized by X-ray and electron diffraction studies and by thermal analysis.

Figure 8a contains the selected area electron diffraction pattern of $LiMoS_2$ oxidized with Br_2 in acetonitrile (MeCN). If $LiMoS_2$ is first exfoliated in water, then rinsed with acetonitrile, forming $Li_{1-n}(MeCN)_xMoS_2$ ($n = 0.75-0.85$), and subsequently oxidized with Br_2 in acetonitrile, similar patterns can be observed. The pattern resembles the one found for the sample $Ba_{0.08}MoS_2$, in which a hexagonal array of diffraction spots

(28) (a) Gash, A. E.; Spain, A. L.; Dysleski, L. M.; Flashenreim, C. J.; Kalaveshi, A.; Dorhout, P. K.; Strauss, S. H. *Environ. Sci. Technol.* **1998**, *32*, 1007−1012. (b) Dorhout, P. K.; Strauss, S. H. In *ACS Symposium Series: Inorganic Materials Synthesis New Directions for Advanced Materials*; Winter, C. E., Ed.; American Chemical Society: Washington, DC, 1999; pp 53−68. (c) Strauss, S. H. In *ACS Symposium Series: Metal Ion Separtion and Preconcentration Progress and Opportunities*; Bond A. H., Dietz, M. L., Rogers, R. D., Eds.; American Chemical Society: Washington, DC, 1999; pp 156−165.

(29) Pinnavaia, T. J. *Science* **1983**, *220*, 365.

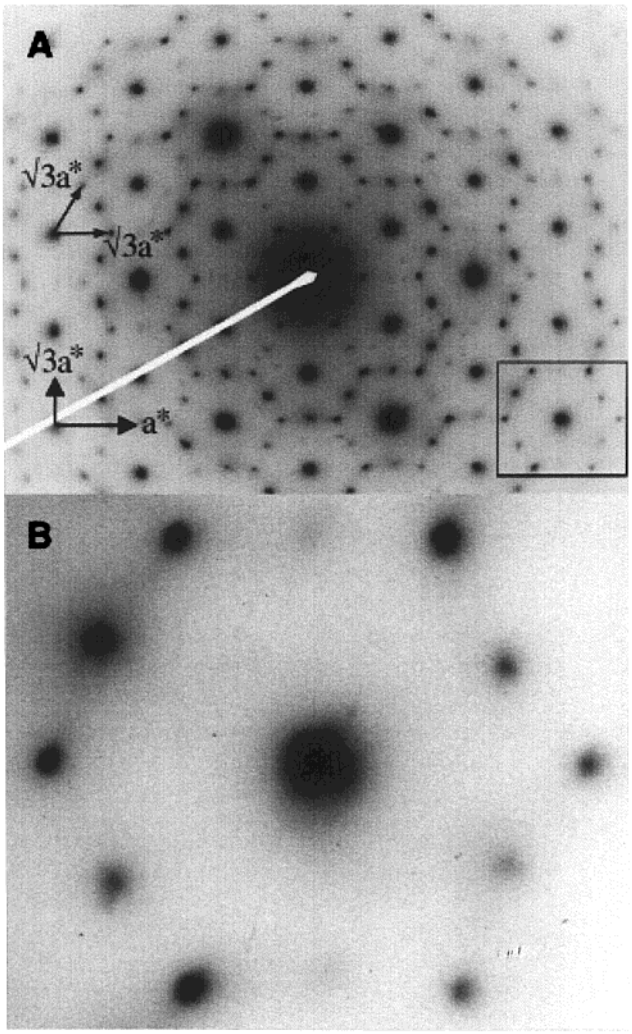

Figure 8. SAED pattern of (A) $LiMoS_2$ oxidized with Br_2 in MeCN. The pattern, which resembles those found in Figure 6, is a combination of twinned $\sqrt{3}a \times a$ orthorhombic lattice and a $\sqrt{3}a \times \sqrt{3}a$ hexagonal lattice of MoS_2. The two lattices have slightly different cell parameters, which results in a distortion of the "honeycomb" as one moves further from the center of the pattern (B).

resembling a "honeycomb" is formed by the superposition of the twinned $\sqrt{3}a \times a$ lattice caused by Mo−Mo distortions and a $\sqrt{3}a \times \sqrt{3}a$ lattice formed by the ordering of the Ba^{2+} cations. The SAED pattern from oxidation of MoS_2 with Br_2 is caused by a superposition of two types of lattices as well; however, in this case the $\sqrt{3}a \times \sqrt{3}a$ lattice is not due to Li^+ cations ordering between the layers, but different Mo−Mo associations. Wypych and co-workers have reported that, upon treatment with I_2 or $K_2Cr_2O_7$, $K_{0.33}(H_2O)_yMoS_2$ is oxidized to a material that contains a $\sqrt{3}a \times \sqrt{3}a$ lattice attributed to Mo−Mo associations.[22a,b] This material has a smaller a parameter than restacked MoS_2. A closer inspection of Figure 8a reveals that the hexagons become increasingly distorted as one moves further away from the center spot (Figure 8b), indicating a mismatch in the two lattices. The $\sqrt{3}a \times \sqrt{3}a$ lattice has a smaller a parameter than the $\sqrt{3}a \times a$ lattice. If $Li_{1-n}(MeCN)_xMoS_2$ is treated with Br_2 it is possible to find electron diffraction patterns of a few crystals which contain only the $\sqrt{3}a \times \sqrt{3}a$ lattice, but the majority of the sample is a decomposition product. The material with the $\sqrt{3}a \times \sqrt{3}a$ lattice is metastable and appears to be more susceptible to conversion to 2H-MoS_2 than the material with the $\sqrt{3}a \times a$ lattice. If one treats $LiMoS_2$ with Br_2 for a longer period of time or with sonication, the $\sqrt{3}a \times \sqrt{3}a$ lattice disappears, leaving a mixture of 2H-MoS_2 and material with the $\sqrt{3}a \times a$ lattice.

The electron diffraction patterns of WS_2 samples obtained upon oxidation with Br_2 are different from those of MoS_2 samples. Almost all patterns contained only the original $\sqrt{3}a \times a$ lattice, even with repeated sonication and stirring in excess Br_2 for a week. After a week a small amount of 2H-WS_2 could be found, and the amount of diffuse scattering was significantly increased due to decomposition to amorphous product(s). From these results one can conclude that either the product has not been oxidized or restacked WS_2 does not exhibit an alternate superlattice upon oxidation. Although the majority of the product exhibited no change, in almost every sample examined there was a small minority of crystallites which gave rise to a diffraction pattern that could be indexed as a $2\sqrt{3}a \times 2\sqrt{3}a$ lattice. This suggests that even if WS_2 is able to have an alternate superlattice upon oxidation it is not the same as the lattice found in oxidized MoS_2.

X-ray Diffraction Studies of Oxidized MS_2. $LiMS_2$ and $Li_{1-n}(MeCN)_xMS_2$ were also examined by transmission X-ray diffraction (Figures 9 and 10). Due to the turbostratic nature of these samples induced by the exfoliation/flocculation process, only $hk0$ reflections are visible from the $\sqrt{3}a \times a$ lattice. Interpretation of the X-ray diffraction patterns is more difficult than that of the electron diffraction patterns in part because the peaks are broad. Furthermore, some $h0l$ reflections of the 2H form of the dichalcogenide overlap with the unique $hk0$ reflections from the $\sqrt{3}a \times a$ lattice and the $\sqrt{3}a \times \sqrt{3}a$ lattice. For example, the 200 of the $\sqrt{3}a \times \sqrt{3}a$ lattice overlaps with the 103 of 2H-MS_2. In fact, the presence of the $\sqrt{3}a \times \sqrt{3}a$ lattice cannot be reliably determined by powder X-ray diffraction because the only reflection that is not subject to an overlap problem is the 100, which is extremely weak. The presence of the $\sqrt{3}a \times a$ lattice is more easily monitored because the 210, a moderately strong reflection at $d = 2.10$ Å, does not overlap with peaks from either of the other two phases which may be present in the sample.

The time-dependent behavior of the oxidation of restacked MoS_2 (and $LiMoS_2$) is illustrated in Figure 9. Initially the $\sqrt{3}a \times a$ lattice dominates (Figure 9a), with the appearance of a shoulder ($d = 1.56$ Å) on the 130 reflection at $2\theta = \sim 59°$ and a new peak at $2\theta = 35°$ ($d = 2.55$ Å), which is not visible in the electron diffraction patterns and is not readily indexed to any of the 3 phases which may be present. At an intermediate stage a new peak appears at $2\theta = \sim 38°$ ($d = 2.35$ Å) which, as mentioned previously, can be indexed as either the 200 of the $\sqrt{3}a \times \sqrt{3}a$ lattice or the 103 of 2H-MoS_2 (Figure 9b). The 110 and the 130 reflections begin to shift to smaller d spacings ($d = 2.78$ to 2.71 Å and 1.61 to 1.59 Å). This is not surprising, because the $\sqrt{3}a \times a$ lattice has the largest a parameter at 3.21 Å; the $\sqrt{3}a \times \sqrt{3}a$ lattice is slightly contracted, as evidenced by the electron diffraction patterns; and in 2H-MoS_2 $a = 3.16$ Å. The 210 peak of the $\sqrt{3}a \times a$ lattice at $2\theta = \sim 38°$ ($d = 2.10$ Å) is still present, and the shoulder at $2\theta = \sim 59°$ has become more pronounced. In the final stage the diffraction pattern no longer contains the peak at $2\theta = 35°$ ($d = 2.55$ Å) or the 210 peak of the $\sqrt{3}a \times a$ lattice at $2\theta = \sim 38°$ ($d = 2.10$ Å), and the 110 and the 130 reflections have shifted to even smaller d spacings ($d = 2.69$ and 1.58 Å). The pattern at this stage contains mostly MoS_2 that has converted to the 2H form.

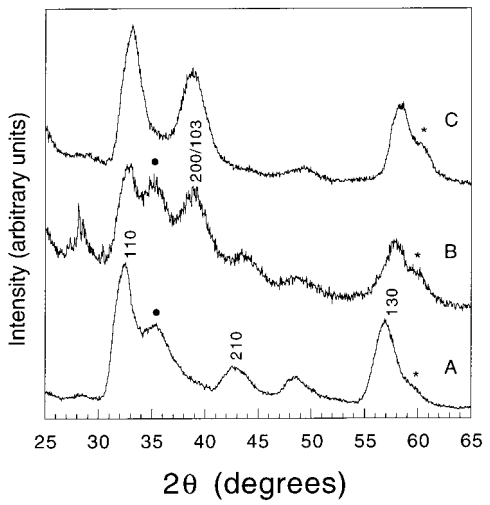

Figure 9. Transmission X-ray diffraction (XRD) pattern of $LiMoS_2$ oxidized in MeCN with increasing time. (A) Initially the pattern contains the $\sqrt{3}a \times a$ lattice with two new peaks at 2.55 Å (solid black circle) and 1.56 Å (asterisk). (B) A peak at 2.3 Å appears, indexed as either the 200 of the $\sqrt{3}a \times \sqrt{3}a$ lattice or the 103 of 2H-MoS_2. (C) The 210 of the $\sqrt{3}a \times a$ lattice has disappeared. The pattern is mostly 2H-MoS_2.

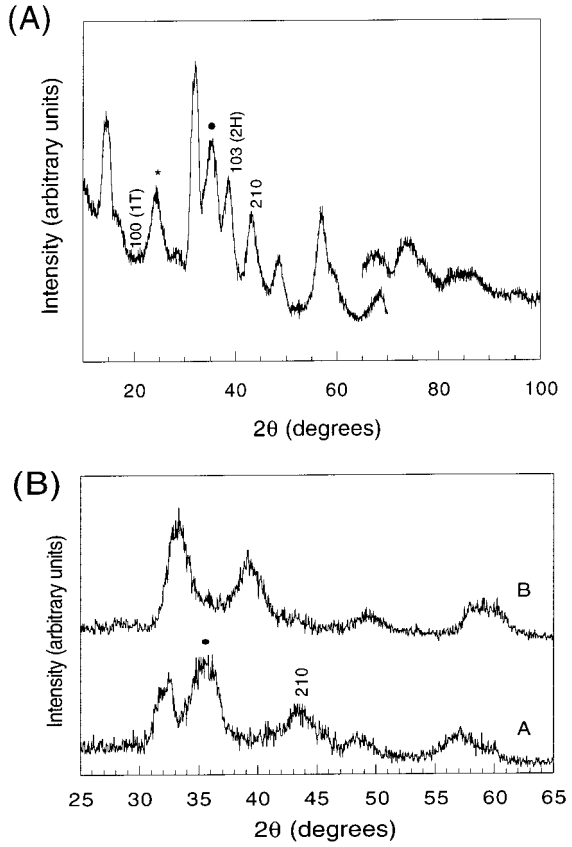

Figure 10. (A) Transmission XRD pattern of $LiWS_2$ oxidized with Br_2 in MeCN. The black circle marks a peak at 2.55 Å which does not appear to be an *hk*0 reflection of any of the three expected lattices. The asterisk marks a contribution from the Saran wrap substrate. (B) Transmission XRD pattern of $LiWS_2$ oxidized with Br_2 before and after heating. The peak at 2.55 Å (black circle) disappears, leaving 2H-WS_2.

The transmission X-ray diffraction patterns of restacked WS_2 (and $LiWS_2$) upon treatment with Br_2 (Figure 10a) resemble those of oxidized restacked MoS_2. The peak at $2\theta = 35°$ ($d = 2.55$ Å) appears but, unlike in MoS_2, does not disappear with time. Under more rigorous conditions or with time the peak at $2\theta = \sim 38°$ ($d = 2.35$ Å) appears. Given that there is no evidence of a $\sqrt{3}a \times \sqrt{3}a$ lattice by electron diffraction, that peak is probably best indexed as the 103 reflection of 2H-WS_2. The disappearance of the 210 peak of the $\sqrt{3}a \times a$ lattice at $2\theta = \sim 38°$ ($d = 2.10$ Å) and the new peak at $2\theta = 35°$ ($d = 2.55$ Å) happens upon heating the material, which converts it to 2H-WS_2 (Figure 10b).

The reflection X-ray diffraction patterns contain the basal 001 reflection at 6.05 Å for WS_2 and 6.21 Å for MoS_2, indicating the deintercalation of most or all of the lithium cations. The basal spacing of WS_2 is slightly contracted (0.1 Å) relative to 2H-MS_2, but expands upon heating.

Residual negative charge on MoS_2 is also substantiated by these diffraction patterns. The structure of restacked MoS_2 and WS_2, which we recently solved from electron diffraction data and found to be WTe_2 type, consists of metal−metal associations to form zigzag chains.[21] As mentioned previously, a material called "1T-MoS_2" has been prepared by the oxidation of $K_{0.33}(H_2O)_yMoS_2$ and found to have a $\sqrt{3}a \times \sqrt{3}a$ lattice by X-ray diffraction and also by STM studies.[22,24] The starting material $K_{0.33}(H_2O)_yMoS_2$, however, has also been studied by STM and found to have the same structural distortion as restacked MoS_2 and WS_2.[30] Furthermore, it is evident by the electron diffraction studies presented here that restacked MoS_2 can be at least partially converted to "1T-MoS_2" upon treatment with Br_2 or I_2. The exterior of the particle appears to be oxidized, forming the $\sqrt{3}a \times \sqrt{3}a$ lattice, whereas the interior of the particle retains the original $\sqrt{3}a \times a$ structure. Actually in their STM studies of 1T-MoS_2 the authors conceded that occasionally they observed the $\sqrt{3}a \times a$ lattice found in their starting material and concluded that it was symptomatic of incomplete oxidation of those samples.

DSC Studies of Oxidized MS_2. As mentioned earlier, restacked MoS_2 and WS_2 are metastable, and can be converted to 2H-MS_2 by an irreversible exothermic transition upon heating. The 1T- form of MoS_2 with the $\sqrt{3}a \times \sqrt{3}a$ lattice has also been reported to be metastable with a comparable conversion.[22] Figure 11a contains a DSC measurement of oxidized MoS_2, which has been identified by electron diffraction to contain both the $\sqrt{3}a \times a$ and $\sqrt{3}a \times \sqrt{3}a$ lattices, and a DSC measurement of restacked MoS_2 for comparison. Restacked MoS_2 undergoes conversion to 2H-MoS_2 at 98 °C (at a heating rate of 5 deg C/min). The transition in the MoS_2 obtained by oxidizing $LiMoS_2$ with Br_2 in acetonitrile occurs at a lower temperature, the broad peak reaching a maximum at 90 °C. Although by TEM it is evident that the material contains more than one kind of lattice, it is not possible to resolve two separate transitions. $Li_{1-n}(MeCN)_xMoS_2$ oxidized with Br_2 converts rapidly, and a DSC measurement of the material could not be obtained.

The situation is different and somewhat more complicated for the oxidation of WS_2 samples (Figure 11b,c). Restacked WS_2 undergoes conversion to 2H-WS_2 at 195 °C (at a heating rate of 5 deg C/min). WS_2 obtained by treating $LiWS_2$ with Br_2 in acetonitrile converts at 149 °C, whereas $Li_{1-n}(MeCN)_xWS_2$ treated with Br_2 in acetonitrile converts at 189 °C. By electron diffraction and transmission X-ray diffraction the materials are structurally identical, containing the $\sqrt{3}a \times a$ lattice. The oxidation was carried out in acetonitrile because aqueous exfoliated WS_2 decomposes fairly rapidly upon exposure to Br_2, but if the aqueous reaction is isolated within a few minutes it is possible to see a shift in the transition to 183 °C. By

(30) Wypych, F.; Weber, Th.; Prins, R. *Surf. Sci. Lett.* **1997**, *380*, L474−478.

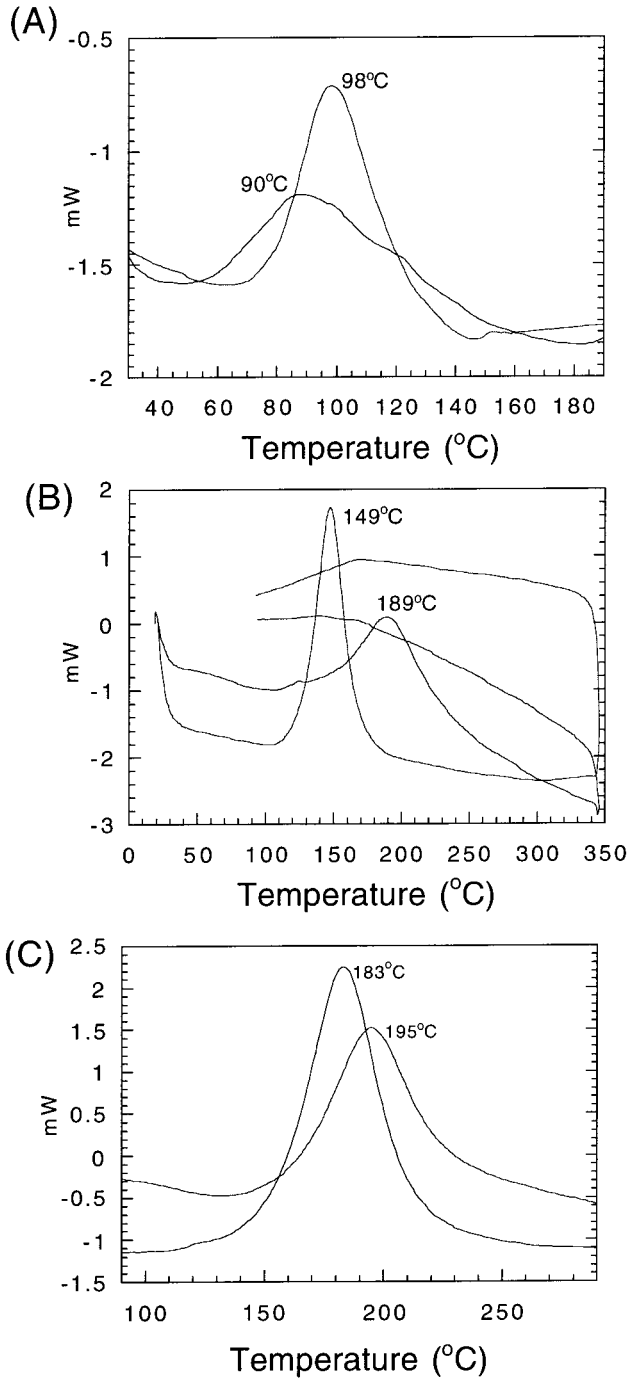

Figure 11. (A) Differential scanning calorimetry (DSC) plots of restacked MoS_2 and $LiMoS_2$ oxidized with Br_2. Restacked MoS_2 exhibits an irreversible exothermic phase transition at 98 °C, corresponding to its conversion to 2H-MoS_2. $LiMoS_2$ oxidized with Br_2 undergoes a similar transition at 90 °C. (B and C) DSC plots showing the irreversible exothermic phase transition to 2H-WS_2. Restacked WS_2 converts at 195 °C; $LiWS_2$ and $Li_{1-n}(MeCN)_xWS_2$ oxidized with Br_2 in MeCN at 149 °C and 189 °C, respectively; and $Li_{1-n}(H_2O)_xWS_2$ oxidized with Br_2 in H_2O converts at 183 °C.

transmission X-ray diffraction this material has the $\sqrt{3}a \times a$ lattice with a small shoulder at 2.55 Å, indicating that it has the same structure as the products of the oxidation of $Li_{1-n}(MeCN)_xWS_2$ and $LiWS_2$.

The structural behavior of restacked WS_2 and $LiWS_2$ is clearly different from that of restacked MoS_2 and $LiMoS_2$ upon treatment with Br_2. Despite the lack of a $\sqrt{3}a \times \sqrt{3}a$ phase in the WS_2 system, there is a dramatic shift in conversion temperature, from 195 to 149 °C, which is reminiscent of the shift in the transition temperature observed in the MoS_2 system. This shift suggests that oxidation has in fact taken place. Furthermore, reflection X-ray diffraction indicates no residual cations between the layers (i.e., the *d* spacing is 6.1 Å). The fact that both restacked and oxidized WS_2 have the $\sqrt{3}a \times a$ lattice implies that, at least in WS_2, the shift in conversion temperature is not dependent on a structural rearrangement, but rather the degree to which the sample is oxidized. The discrepancy in transition temperature between Br_2 treated $LiWS_2$ and Br_2 treated $Li_{1-n}(MeCN)_xWS_2$ is probably due to limited diffusion in $Li_{1-n}(MeCN)_xWS_2$. In $LiWS_2$ the acetonitrile can solvate the lithium cations, swelling the layers apart and allowing the oxidant to access the layers more intimately, whereas $Li_{1-n}(MeCN)_xWS_2$ does not swell in acetonitrile; hence the interior of the particles is inaccessible to the oxidizing agent and the material remains trapped in the incompletely oxidized state that it achieved upon exfoliation in water.

Studies of the structure dependence upon oxidation state in MoS_2 (and WS_2) are complicated in part because 2H-MoS_2 undergoes a phase transition upon lithiation in which the coordination environment changes from trigonal prismatic to octahedral. If only a small amount of lithium is introduced the material can remain in the 2H-MoS_2 structure.[31] It has also been observed that the material does not convert to the octahedral structure homogeneously with small amounts of lithium, resulting in a two-phase system.[18a] Electrochemical studies which start with 2H-MoS_2 are difficult to interpret due to this problem.[32] The $\sqrt{3}a \times a$ octahedral phase (that with the zigzag M−M chains) can be used as a starting point, however. Electrochemical studies of Li_xMoS_2, $K_x(H_2O)_yMoS_2$, and $K_x(H_2O)_yWS_2$ which start from the octahedral structure indicate the presence of 4−6 different phases in the range $x = 0$ to 1.[18b,33] Although some authors have attributed these many phases to cation ordering in the gallery,[32] others have attributed them to charge density waves.[33] The different observed superlattices in MoS_2 suggest that charge density waves are responsible for at least some of these phases. Wypych and co-workers have proposed a scheme containing three different lattices: a $2a \times 2a$ for $K_{0.7}MoS_2$, $\sqrt{3}a \times a$ for $K_{0.33}(H_2O)_yMoS_2$, and a $\sqrt{3}a \times \sqrt{3}a$ for 1T-MoS_2.[24] A comparison of the electrochemical behavior of $K_x(H_2O)_yMoS_2$ and $K_x(H_2O)_yWS_2$ reveals that the two materials behave differently at low *x* values,[33] consistent with the different electron diffraction results observed in the oxidation of $LiMoS_2$ and $LiWS_2$ with Br_2.

Acid Restacked MS_2. When $LiMS_2$ is exfoliated in concentrated acid the product should form a proton bronze, H_xMS_2. The transmission X-ray diffraction patterns for the reaction of $LiMoS_2$ and $LiWS_2$ with concentrated HCl (Figure 12a) show that the materials retain the $\sqrt{3}a \times a$ lattice and a peak appears at 2.55 Å. The products were examined by electron diffraction and exhibited only the $\sqrt{3}a \times a$ lattice with no evidence of an additional reflection at 2.55 Å. In this case, the structure of H_x-MoS_2 is the same as that of H_xWS_2, exhibiting no evidence of a $\sqrt{3}a \times \sqrt{3}a$ lattice. The reflection X-ray diffraction patterns exhibit basal 00*l* spacings of 6.05 Å.

If $LiWS_2$ is exfoliated directly in concentrated HCl the DSC

(31) Papageorgopoulos, C. A.; Jaegermann, W. *Surf. Sci.* **1995**, *338*, 83−93.

(32) Julien, C. Lithium Insertion in Chalcogenides: Electrochemical Properties and Electrode Applications. In *Microionics: Solid State Integrable Batteries*; Balkanski, M., Ed.; Elsevier Science: New York, 1991; pp 309−341.

(33) Wypych, F.; Sollmann, K.; Schöllhorn, R. *Mater. Res. Bull.* **1992**, *27*, 545−553.

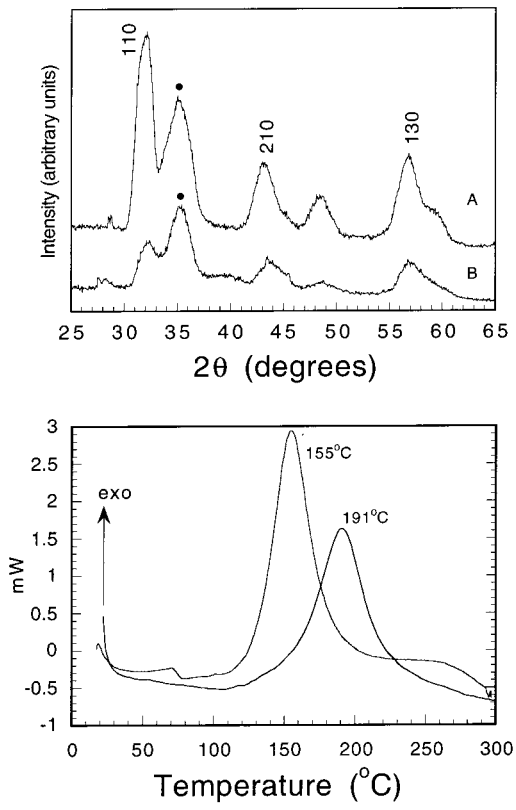

Figure 12. (A) Transmission XRD patterns of H_xWS_2 and H_xMoS_2 obtained from $LiMS_2$ exfoliated in concentrated HCl. Black circle marks peak at 2.55 Å. (B) DSC plots of H_xWS_2 obtained from the reaction of HCl with $LiWS_2$ (155 °C) and $Li_{1-n}(H_2O)_xWS_2$ (191 °C).

shows an exothermic transition at 155 °C, whereas if it is first exfoliated in H_2O and then concentrated acid is added it exhibits a transition temperature of 191 °C (Figure 12b). Presumably the x values in the products of each reaction, H_xWS_2, are different. The discrepancy in the behavior of $LiWS_2$ and $Li_{1-n}(H_2O)_xWS_2$ in acidic conditions is similar to the discrepancy upon oxidation with Br_2, in which the difference in conversion temperatures could be attributed to a diffusion problem. Exfoliation in concentrated acid provides more oxidizing conditions than exfoliation in H_2O before addition of acid. The amount of oxidation during the exfoliation process is important because there is a competition between oxidation and proton encapsulation. Once the material has flocculated its oxidation is limited by diffusion, hence the discrepancy in transition temperatures.

$LiMoS_2$ exfoliated in concentrated acid does not exhibit a shift in its exothermic transition to a lower temperature. The structure of H_xMoS_2 samples prepared from the reaction of $LiMoS_2$ and $Li_{1-n}(H_2O)_xMoS_2$ with acid resembles that of their W analogues more than in Br_2 solution. There is no evidence of the $\sqrt{3}a \times \sqrt{3}a$ phase in acidic conditions. This suggests that the hypothesis of Golub et al. that MoS_2 is fully oxidized upon treatment with acid is not correct, only that protons are now the encapsulated counterion.[17]

As mentioned previously, the authors who first reported the exfoliation of MoS_2 believed that the negative charge of the layers was due to OH^- groups associated with the basal planes of the layers. It was believed that exfoliated MoS_2 (and WS_2) has a point of zero charge (PZC) upon acidification. The authors used the different PZC to create a restacked composite material with alternating MoS_2 and WS_2 layers, forming a superstructure along the 00l axis.[16c] Their evidence for a superstructure of alternating MoS_2 and WS_2 layers was poor. A better interpretation of these results is that the introduction of protons to a homogeneous mixture of exfoliated layers resulted in rapid flocculation, creating a homogeneous mixture of MoS_2 and WS_2 in the product. They also suggested that PZC occurs at slightly different pH for the edge OH^- sites and basal OH^- sites, and used this to create a house-of-cards structure for MoS_2.[16b] The evidence for this kind of structure was the low intensity of the 00l reflections in the X-ray diffraction pattern. However, the intensity of the 00l reflections, which is indicative of the degree of order in the flocculated layers, can be influenced by a variety of factors (the ionic strength of the solution, for example), and does not constitute proof of a point of zero charge on the layers.

The peak at 2.55 Å in the transmission X-ray diffraction patterns of H_xMS_2 and $LiMS_2$ oxidized with Br_2 is puzzling, but shifting of the layers relative to one another could allow $h0l$ reflections to appear. A 102 reflection has been observed in some samples of 2H-MoS_2 at that d spacing. The peak at 2.3 Å is almost certainly the 103 of 2H-MS_2.

An illustration of the different superlattices observed in MoS_2 and WS_2 due to M−M associations can be found in Figure 13. An ideal 1T-MS_2 lattice (not experimentally observed) can distort to form zigzag chains, giving rise to the orthorhombic $\sqrt{3}a \times a$ lattice found in restacked MoS_2 and WS_2. It can trimerize, giving rise to a $\sqrt{3}a \times \sqrt{3}a$ lattice found in MoS_2 upon oxidation with Br_2 or I_2 (Figure 13c). Finally, when WS_2 is treated with Br_2, a minority phase with a $2\sqrt{3}a \times 2\sqrt{3}a$ lattice is formed. This distortion could be due to a number of M−M associations, perhaps a trimerization similar to Figure 13c or a tetramerization (Figure 13d).

One question that arises from the behavior of restacked MoS_2 upon treatment with Br_2 is, why does restacked MoS_2, a d^{2+n} system, prefer a $\sqrt{3}a \times a$ distortion, whereas oxidized restacked MoS_2 adopts a $\sqrt{3}a \times \sqrt{3}a$ distortion? Also, is oxidized restacked MoS_2 a precisely d^2 system, or a d^{2+x} system ($0 < x < n$)? To address these questions, we have investigated the electrical properties of restacked MoS_2 and WS_2.

Thermopower Measurements. As mentioned previously, the reduction of 2H-MoS_2 with lithium results in a structural transformation from trigonal prismatic to octahedral metal coordination and a change in properties from semiconducting to metallic. These changes have been explained using a depiction of the band structures for $LiMoS_2$ in both coordination environments, which illustrates a net stabilization in energy upon conversion to octahedral giving a half-filled band with predominantly d orbital character.[18]

Restacked MoS_2 and WS_2 retain octahedral coordination about the metal atom,[21] and their conductivity has been reported elsewhere[4,7b] to be metallic. If one simply removes electrons from the half-filled band which was published for $LiMoS_2$, an idealized octahedral d^3 system, one should expect an n-type conductor for the d^2 system (Figure 14b). Thermopower measurements on restacked MoS_2 and WS_2, however, indicate that they are p-type (hole) conductors (Figure 14a), with room temperature values of 50 and 20 μV/K, respectively. The structural distortion in restacked MoS_2 and WS_2 to form zigzag chains obviously should result in a change in the band structure. In fact, distortion of octahedral ML_2 d^2 systems to form zigzag chains has been predicted by extended Hückel tight binding calculations[34] and, for a precisely d^2 system, results in a half-filled band (Figure 14a). If, however, the system is actually d^{2+n}, as is the case with restacked MoS_2 and WS_2, residual negative

(34) (a) Rovira, C.; Whangbo, M.-H. *Inorg. Chem.* **1993**, *32*, 4094. (b) Whangbo, M.-H.; Canadell, E. *J. Am. Chem. Soc.* **1992**, *114*, 9587.

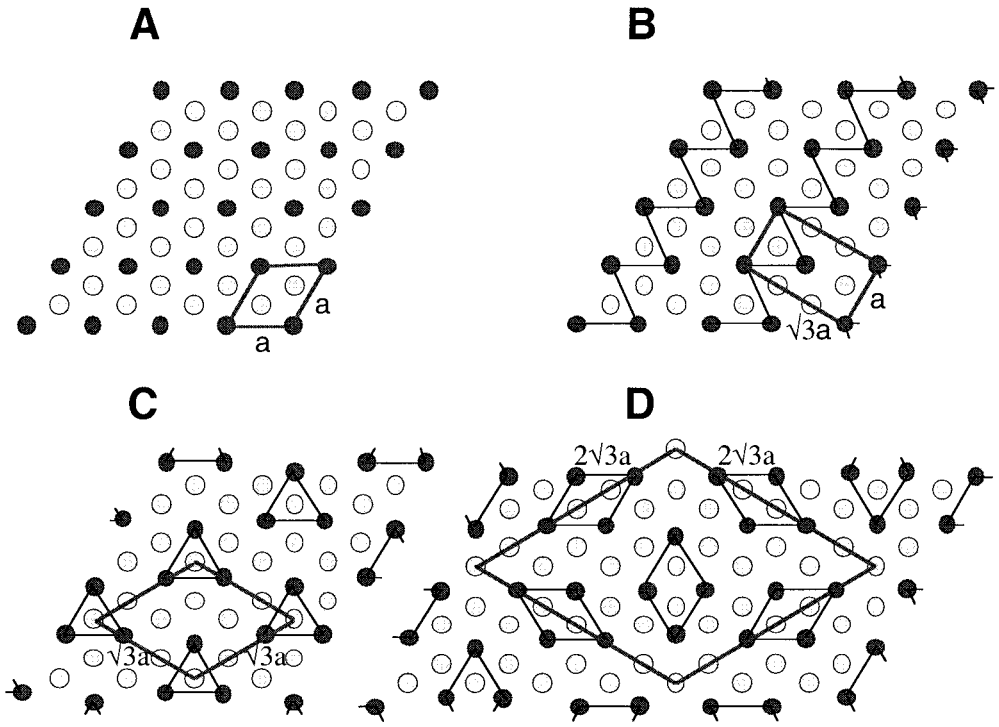

Figure 13. Schematic illustrating (A) an ideal 1T-MS_2 lattice, (B) a $\sqrt{3}a \times a$ lattice with infinite zigzag metal chains, (C) a $\sqrt{3}a \times \sqrt{3}a$ lattice with trimers, and (D) a $2\sqrt{3}a \times 2\sqrt{3}a$ lattice with possible tetramers formed due to M−M distortions.

charge results in a more than half-filled band and consequently p-type conductivity, consistent with our experimental observations.

The effects of M−M trimerization on the band structure of d^2 ML_2 systems have also been explored, and it has been predicted that even a very small displacement of the metal atoms (0.023 Å) results in the opening of a band gap at the Fermi level.[34] $LiVO_2$, a d^2 system that exhibits a $\sqrt{3}a \times \sqrt{3}a$ superstructure, has an experimentally observed band gap of 0.1−0.2 eV.[35] This suggests that a precisely d^2 system is required for a $\sqrt{3}a \times \sqrt{3}a$ superstructure resulting from M−M trimerization; otherwise, the gap opened at the Fermi level due to the structural distortion is destroyed. The zigzag chain distortion, however, does not result in a band gap, and therefore can accommodate some residual negative charge. It should be noted that, in the original publication which reported a $\sqrt{3}a \times \sqrt{3}a$ superstructure for MoS_2, metallic behavior was mentioned.[22a] However, subsequent STM studies indicated that samples are susceptible to contamination with incompletely oxidized material that contains the $\sqrt{3}a \times a$ superstructure.[24]

Conclusions

MoS_2 and WS_2 retain some negative charge upon exfoliation and flocculation. Although it is possible to incorporate neutral species, cations can also be encapsulated without a detectable co-encapsulated anion, usually giving rise to very ordered reflectance X-ray diffraction patterns.[9−13,17] In the studies presented here hard, electropositive alkali cations have been encapsulated in MoS_2 and WS_2 under neutral synthetic conditions. The choice of these cations and these synthetic conditions minimizes the risk of co-encapsulation of OH^- ions. The cations order in the gallery, forming additional superlattices. The range of negative charge on the layers appears to be 0.15−0.25 for both MoS_2 and WS_2, which is consistent with measurements on samples prepared in a similar fashion by other researchers.[17]

Structural characterization of restacked MoS_2 also supports a negative charge. Restacked MoS_2 and WS_2 have been found by electron diffraction to have the same superlattice as $K_x(H_2O)_y$-MoS_2.[21,24] Treatment of restacked MoS_2 with Br_2 results in a change from a $\sqrt{3}a \times a$ superlattice to a $\sqrt{3}a \times \sqrt{3}a$ superstructure, which is analogous to the superstructure observed in "1T-MoS_2", the oxidation product of $K_{0.7}MoS_2$.[22] This change in structure upon exposure to an oxidizing agent implies that restacked MoS_2 is incompletely oxidized, and is probably better formulated as Li_xMoS_2 or $Li_x(H_2O)_yMoS_2$.

Restacked WS_2 does not appear to exhibit a structural change upon exposure to Br_2. However, both restacked MoS_2 and WS_2 exhibit irreversible exothermic transitions which are shifted to lower transition temperatures upon treatment with Br_2. The shift is quite significant in WS_2, from 195 to 149 °C in the Br_2-treated sample, indicating that oxidation has taken place. It is somewhat surprising, however, that oxidation of restacked WS_2 does not result in an alternate superlattice analogous to the $\sqrt{3}a \times \sqrt{3}a$ superstructure observed in oxidized MoS_2. The products of all thermal conversions are the semiconducting phase 2H-MS_2, which requires an expulsion of the residual negative charge and explains why the oxidation state affects the transition temperature. The expulsion of the residual negative charge likely results in the reduction of residual H_2O (or H^+ in H_xMS_2), forming H_2 gas.[36]

The different phases of MoS_2 produced under various experimental conditions are illustrated in Figure 15a. This scheme is intended to correlate all forms of MoS_2 and the interconversion between forms, and to help clear up any remaining confusion regarding the nature of this system. Exfoliation and flocculation of $LiMoS_2$ in water results in

(35) (a) Takei, H.; Koike, M.; Imai, K.; Sawa, H.; Kadowaki, H.; Iye, Y. *Mater. Res. Bull.* **1992**, *27*, 555. (b) Imai, K.; Sawa, H.; Koike, M.; Hasegawa, M.; Takei, H. *J. Solid State Chem.* **1995**, *114*, 184.

(36) Proton NMR studies of the gaseous species released upon conversion of restacked MoS_2 to 2H-MoS_2 indicated the presence of hydrogen gas. Heising, J.; Kanatzidis, M. G. Unpublished results.

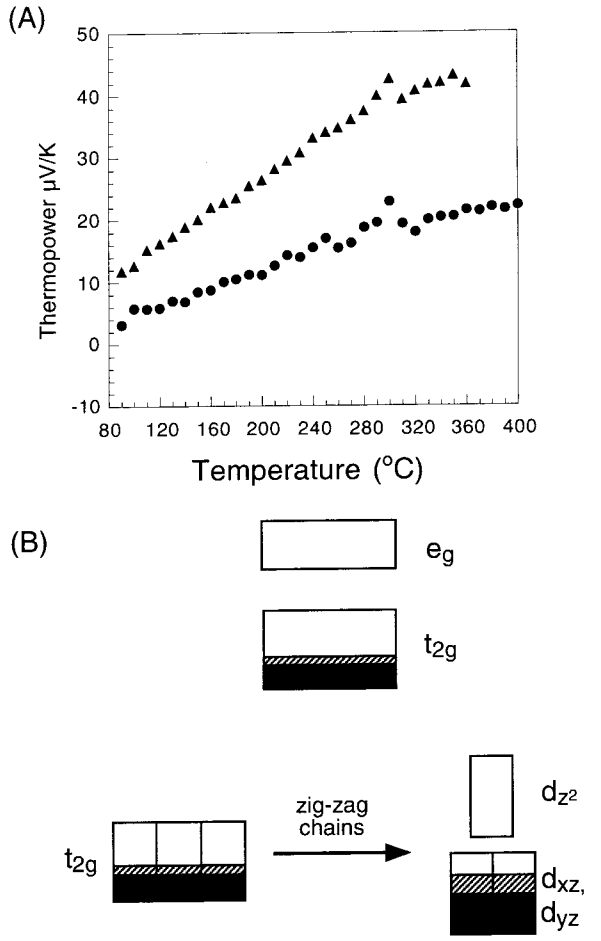

Figure 14. (A) Thermopower measurements of restacked MoS_2 (triangles) and WS_2 (circles). The relatively small magnitude and slope of the data is consistent with that of a p-type metallic conductor. (B) Schematic band diagram illustrating the distortion of an ideal octahedral system to form zigzag chains. The ideal system describes an n-type conductor whether it is d^2 (black fill) or d^{2+x} (black fill + stripes). The distorted system is half filled for d^2 and more than half filled for d^{2+x}, resulting in a p-type metallic conductor.

restacked MoS_2, which can be more accurately formulated as $Li_{0.2}MoS_2$ (**2**) based on the chemical analyses of the alkali cation encapsulated products. Oxidation of $LiMoS_2$ in Br_2/MeCN results in a mixture of "1T-MoS_2" (**3**) and $Li_{0.2}MoS_2$. $LiMoS_2$ exfoliated in H_2O can be converted to the same mixture upon treatment with Br_2/MeCN. If $LiMoS_2$ is exfoliated in concentrated HCl it forms H_xMoS_2, a material with the same superstructure as $Li_{0.2}MoS_2$ which does not appear to be oxidized. A similar scheme in Figure 15b illustrates the analogous phases of WS_2. A principal difference is that the product of the oxidation of $LiWS_2$ with Br_2 in MeCN, called "WS_2" (**3**), is not structurally different from $Li_{0.2}WS_2$. Depending on the preparation, it is possible to isolate products exhibiting a continuum of transition temperatures between 149 °C and the transition temperature of $Li_{0.2}WS_2$ (195 °C). Another difference is that, unlike in MoS_2, when $LiWS_2$ reacts with concentrated HCl, the transition temperature of the product (155 °C) is closer to that of the oxidized material (**3**) rather than $Li_{0.2}WS_2$. Given

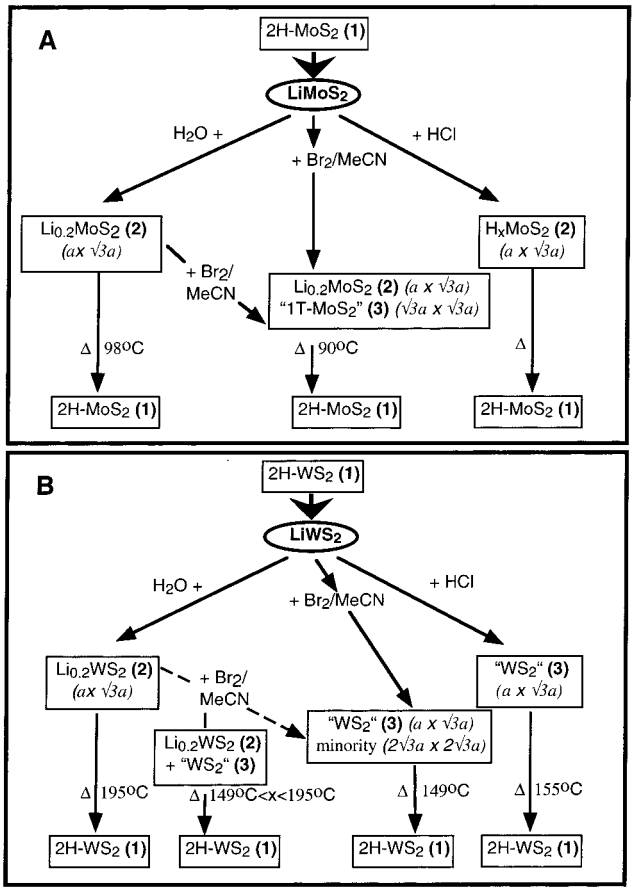

Figure 15. Reaction scheme illustrating the different phases obtained with various treatment of (A) MoS_2 and (B) WS_2.

the higher energy of the d orbitals of W, it is not surprising that WS_2 is more readily oxidized than MoS_2 under comparable experimental conditions.

Clearly the MoS_2 and WS_2 systems are rather complicated, and the nature of the phase obtained is very sensitive to the experimental conditions used to prepare the product. The term "restacked MoS_2" has been used casually in the literature to represent material that has been converted to the 2H form as well as the metastable compound with the $\sqrt{3}a \times a$ lattice, and is usually written without a formulation of the negative charge present. In addition, MoS_2 and WS_2 resemble one another, but there are distinct differences between the two systems. To prevent future confusion researchers should take special care to formulate their products precisely, and also to recognize that restacked MoS_2 (and WS_2) which has been heated above its conversion temperature is better described by the formula 2H-MoS_2 (and 2H-WS_2).

Acknowledgment. Financial support from the National Science Foundation CHE 96-33798 (Chemistry Research Group) is gratefully acknowledged. This work made use of the SEM and TEM facilities at the Center for Electron Optics at Michigan State University. Thanks to Dr. John Heckman and Professor T. J. Pinnavaia for fruitful discussions and Dr. Duck-Young Chung for thermopower measurements.

JA991644D